


Article

Strongly Interacting Bose Polarons in Two-Dimensional Atomic Gases and Quantum Fluids of Polaritons

Luis Fernando Cárdenas-Castillo¹ and Arturo Camacho-Guardian^{2,*} ¹ Facultad de Ciencias, Universidad Nacional de Ingeniería, Lima 15333, Peru; lcardenasc@uni.pe² Departamento de Física Química, Instituto de Física, Universidad Nacional Autónoma de México, Mexico City 04510, Mexico

* Correspondence: acamacho@fisica.unam.mx

Abstract: Polarons are quasiparticles relevant across many fields in physics: from condensed matter to atomic physics. Here, we study the quasiparticle properties of two-dimensional strongly interacting Bose polarons in atomic Bose–Einstein condensates and polariton gases. Our studies are based on the non-self consistent T-matrix approximation adapted to these physical systems. For the atomic case, we study the spectral and quasiparticle properties of the polaron in the presence of a magnetic Feshbach resonance. We show the presence of two polaron branches: an attractive polaron, a low-lying state that appears as a well-defined quasiparticle for weak attractive interactions, and a repulsive polaron, a metastable state that becomes the dominant branch at weak repulsive interactions. In addition, we study a polaron arising from the dressing of a single itinerant electron by a quantum fluid of polaritons in a semiconductor microcavity. We demonstrate the persistence of the two polaron branches whose properties can be controlled over a wide range of parameters by tuning the cavity mode.

Keywords: polaron; exciton–polariton; Feshbach resonance



Citation: Cárdenas-Castillo, L.F.; Camacho-Guardian, A. Strongly Interacting Bose Polarons in Two-Dimensional Atomic Gases and Quantum Fluids of Polaritons. *Atoms* **2023**, *11*, 3. <https://doi.org/10.3390/atoms11010003>

Academic Editors: Luis Aldemar Peña Ardila and Cesar Cabrera

Received: 17 October 2022

Revised: 12 December 2022

Accepted: 22 December 2022

Published: 29 December 2022



Copyright: © 2022 by the authors. Licensee MDPI, Basel, Switzerland. This article is an open access article distributed under the terms and conditions of the Creative Commons Attribution (CC BY) license (<https://creativecommons.org/licenses/by/4.0/>).

1. Introduction

The concept of the polaron initially introduced by Landau and Pekar to describe the motion of an electron in a solid [1,2] has been used in many fields in physics. The quantum motion of an impurity renewed interest in the context of cold atomic gases and allowed for the study of the polaron in uncharted territories. The experimental realization of the so-called Fermi polaron [3–14] in two- and three-dimensions, followed by their three-dimensional counterpart, Bose gas, dramatically improved our understanding of the polaron far beyond the regimes accessible in previous solid-state platforms. These studies include the experimental realization of the Bose polaron in the presence of a Feshbach resonance [15–17], the dynamical formation of the polaron [18], and critical aspects of the polaron [19]. The nature of the strongly interacting polaron unveiled a plethora of phenomena [20–34], paving the way for the study of the Bose polaron beyond the single impurity limit [35–46], dipolar polarons [47], and charged polarons in the atomic context [48–52], among others.

The arrival of semi-conductor microcavities provided new opportunities to explore many-body physics in the quantum degenerate regime. These systems exploit the strong coupling between cavity photons and excitons, in which a new quasi-particle coined polariton may emerge [53]. The study of polaritons has produced spectacular results in physics including the observation of Bose–Einstein condensation [54–56], quantum vortices [57–60], polaritonic Feshbach resonances [61], and stands as a promising field for the control and manipulation of strongly interacting photons. In semiconductor microcavities, new classes of polarons may arise, where the role of the polaron is played by an individual optical excitation dressed by its bath. These aforementioned polarons have received attention allowing for the development of polaron-based lasers [62] and the study of polariton–polariton interactions [63–66]. The polaron–polariton, a quasiparticle resulting from the

dressing of a polariton by its surroundings, has been experimentally realised in the context of the Fermi [67] and Bose polaron-polariton [61]. Despite the intrinsic interest in two-dimensional polaron-polaritons, most theoretical efforts have been devoted to research concerning Fermi polaron excitons [68–74], and Fermi exciton–polaritons [75–78]. Fewer efforts have been directed to the Bose polaron-polariton [79–85].

In the context of ultracold quantum gases, the three-dimensional Bose polaron has received the most theoretical attention, and only a few studies within a mean-field approach [86] and the Fröhlich Hamiltonian for weak interactions [87,88] have addressed the two-dimensional Bose polaron. Only recently, the two-dimensional Bose polaron for strong interactions has been studied using quantum Monte Carlo techniques, unveiling the role of strong correlations in the formation of the Bose polaron [89]. Beyond homogeneous polarons, a new class of strongly interacting two-dimensional polarons arises in the presence of lattice confinement [90]. Nevertheless, many aspects and features of the two-dimensional polaron remain to be understood. Furthermore, in the field of semiconductor microcavities, intriguing predictions of polariton-mediated superconductivity hinge on our ability to understand and enhance the coupling between free carriers (electrons) to polariton condensate modes [91–95]. Understanding of the limit of a single carrier coupled to a polariton BEC is naturally one of the first steps towards this goal.

In this work, we study the spectral properties of strongly interacting impurities in two-dimensional atomic Bose–Einstein condensates and polariton quantum gases. The rest of the paper is organized as follows. First, in Section 2 we study the two-dimensional Bose polaron in an atomic Bose–Einstein condensate. We start by introducing the system and our formalism based on the non-self consistent T-matrix approximation (NSCT) which allows us to study the quasiparticle properties in a non-perturbative manner and treat strong interactions arising from the atomic Feshbach resonances. We then numerically study the zero-momentum properties of the polaron from an NSCT approach, revealing the presence of two polaron states: an attractive and a repulsive quasiparticle. In Section 3, we extend the theoretical approach to consider a highly population-imbalanced Fermi–Bose mixture in a two-dimensional semiconductor microcavity where a polariton condensate is coupled to a minority of itinerant electrons. In this case, we explore the Feshbach physics by varying the cavity detuning to analyze the interplay between light–matter and matter–matter interactions. Finally, in Section 4 we conclude the paper and provide an overview of new challenges regarding the Bose polaron in 2D.

2. The Polaron in a Two-Dimensional Atomic Bose–Einstein Condensate

2.1. System

We start our study considering a single impurity coupled to a two-dimensional atomic Bose–Einstein condensate. This system can be realized experimentally by preparing a highly population-imbalanced Bose–Bose [16] or a Fermi–Bose mixture [15], where a majority BEC hosts few bosonic or fermionic impurities.

The Hamiltonian of the system is taken as $\hat{H} = \hat{H}_B + \hat{H}_c + \hat{H}_I$, where

$$\hat{H}_B = \sum_{\mathbf{k}} \epsilon_{\mathbf{k}}^{(B)} \hat{b}_{\mathbf{k}}^\dagger \hat{b}_{\mathbf{k}} + \frac{g_{BB}}{2\mathcal{A}} \sum_{\mathbf{k}, \mathbf{k}', \mathbf{q}} \hat{b}_{\mathbf{k}+\mathbf{q}}^\dagger \hat{b}_{\mathbf{k}'-\mathbf{q}}^\dagger \hat{b}_{\mathbf{k}'} \hat{b}_{\mathbf{k}}, \tag{1}$$

denotes the Hamiltonian of the majority bosons. Here, $\hat{b}_{\mathbf{k}}^\dagger$ creates a boson with momentum \mathbf{k} and energy $\epsilon_{\mathbf{k}}^{(B)} = k^2/2m_B$ of mass m_B , and g_{BB} the boson-boson interaction strength. Finally, \mathcal{A} denotes the area of the surface. Here, we use periodic boundary conditions. We take $\hbar = 1$.

We assume a weakly interacting BEC described by the Bogoliubov theory, such that the Hamiltonian in Equation (1) can be approximated by

$$\hat{H}_B = \sum_{\mathbf{k}} \omega_{\mathbf{k}} \hat{\beta}_{\mathbf{k}}^\dagger \hat{\beta}_{\mathbf{k}},$$

where $\hat{\beta}_{\mathbf{k}}^\dagger$ creates a Bogoliubov mode with energy $\omega_{\mathbf{k}} = \sqrt{\epsilon_{\mathbf{k}}^{(B)}(\epsilon_{\mathbf{k}}^{(B)} + 2ng_{BB})}$. Here, the density of the BEC is denoted by n .

The non-interacting term of the impurity's Hamiltonian is $\hat{H}_c = \sum_{\mathbf{k}} \epsilon_{\mathbf{k}}^{(c)} \hat{c}_{\mathbf{k}}^\dagger \hat{c}_{\mathbf{k}}$, with $\epsilon_{\mathbf{k}}^{(c)} = k^2/2m_I$ and m_I is the mass of the impurity. Finally, the interaction between the host atoms and the impurity is assumed short-ranged and well-characterized by a contact-interaction. The term accounting for the impurity–boson interactions is

$$\hat{H}_I = \frac{g}{\mathcal{A}} \sum_{\mathbf{k}, \mathbf{k}', \mathbf{q}} \hat{b}_{\mathbf{k}+\mathbf{q}}^\dagger \hat{c}_{\mathbf{k}'-\mathbf{q}}^\dagger \hat{c}_{\mathbf{k}'} \hat{b}_{\mathbf{k}}, \tag{2}$$

where g gives the boson-impurity interaction strength. In two dimensions, the contact interaction supports a two-body bound state whose energy $\epsilon_B < 0$ can be varied on demand with a Feshbach resonance [96]. The coupling strength g and the energy of the bound state are not independent and can be linked via the equation

$$mg = \left[\frac{1}{4\pi} \ln \left(\frac{\epsilon_B}{\epsilon_B - \Lambda^2} \right) \right]^{-1} \approx \left[\frac{1}{4\pi} \ln \left(\frac{\epsilon_B}{-\Lambda^2} \right) \right]^{-1}, \tag{3}$$

where we have assumed equal masses $m = m_B = m_I$ and introduced Λ , an energy cut-off for the impurity-boson interaction. This parameter is assumed to be by far the largest energy scale of the system. As we will show, our results are independent of Λ . It is also convenient to introduce the two-dimensional scattering length defined as $a_{2D} = \sqrt{-2m\epsilon_B}$, a dimensionless parameter $\alpha = \ln(k_n a_{2D})$, a wavevector $k_n = (4\pi n)^{1/2}$, and a typical energy scale of the system defined as $E_n = k_n^2/2m_B$. A quasi-2D geometry in ultracold gases can be created by tightly confining the Bose gas in one direction with a 1D optical lattice. Finally, in typical experiments with ultracold gases [11,16], the minority atoms can be regarded as impurities for concentrations around $n_I/n \lesssim 0.1 - 0.3$, where n_I is the density of the impurities.

To theoretically study the system, we introduce the imaginary-time Green's function for the impurity [97]

$$\mathcal{G}(\mathbf{k}, \tau) = -\langle T_\tau \{ \hat{c}_{\mathbf{k}}(\tau) \hat{c}_{\mathbf{k}}^\dagger(0) \} \rangle, \tag{4}$$

where τ denotes time and T_τ denotes the time-ordering operator. After Fourier transforming the Green's function from the time to the frequency domain, we write the Dyson's equation for the impurity's Green's function $\mathcal{G}(\mathbf{k}, i\omega_\nu)$ in energy-momentum space

$$\mathcal{G}^{-1}(\mathbf{k}, \omega) = \omega - \epsilon_{\mathbf{k}}^{(c)} - \Sigma(\mathbf{k}, \omega), \tag{5}$$

where $\Sigma(\mathbf{k}, \omega)$ is the self-energy of the impurity. We consider all quantities evaluated at real frequencies obtained by analytic continuation $i\omega_\nu \rightarrow \omega + i0^+$, with ω_ν a Matsubara frequency [97].

The excitations can be studied from the spectral function defined as

$$A(\mathbf{k}, \omega) = -2\text{Im}\mathcal{G}(\mathbf{k}, \omega). \tag{6}$$

Due to the inherent complexity of the system, it is impossible to solve the many-body Hamiltonian exactly. Therefore, we need to appeal to certain approximations. Here, we base our study on the so-called T-matrix approximation for the Bose polaron, first introduced to describe three-dimensional polarons [25]. This approach has been successful in helping explain the first generation of Bose polaron experiments [15–19]. The T-matrix approximation can be regarded as a mean-field-like approximation where the mean-field correction ng is replaced by an in-medium scattering matrix

$$\Sigma(\mathbf{k}, \omega) = n\Gamma(\mathbf{k}, \omega), \tag{7}$$

with the in-medium scattering matrix defined as

$$\Gamma^{-1}(\mathbf{k}, \omega) = \frac{1}{g} - \Pi(\mathbf{k}, \omega), \tag{8}$$

to account for repeated impurity-boson scattering within the ladder approximation. This approach only contains normal BEC propagators and accounts for the Feshbach physics. This formalism can be extended in order to include polariton–polariton interactions and also usually requires anomalous BEC functions [38]. One should recall that in the limit of a single boson, the scattering matrix gives an exact solution to the two-body scattering problem between a boson and an impurity [96]. In the ladder approximation, the pair-propagator is given by

$$\Pi(\mathbf{k}, \omega) = - \sum_{q, i\omega_v} \mathcal{G}^{(0)}(\mathbf{q}, i\omega_v) G_{11}(\mathbf{q} + \mathbf{k}, i\omega_v + \omega), \tag{9}$$

where, the BEC Green’s function is given by

$$G_{11}(\mathbf{k}, \omega) = \frac{u_{\mathbf{k}}^2}{\omega - \omega_{\mathbf{k}}} - \frac{v_{\mathbf{k}}^2}{\omega + \omega_{\mathbf{k}}}, \tag{10}$$

with the Bogoliubov mode wavefunctions

$$u_{\mathbf{k}}^2 = \frac{1}{2} \left(\frac{\epsilon_{\mathbf{k}}^{(B)} + n g_{BB}}{\omega_{\mathbf{k}}} + 1 \right),$$

and $u_{\mathbf{k}}^2 - v_{\mathbf{k}}^2 = 1$.

In this study, we employ the non-self consistent T-matrix approximation (NSCT) which consists of taking in Equation (9) the bare impurity propagator

$$\mathcal{G}^{(0)}(\mathbf{k}, \omega) = \frac{1}{\omega - \epsilon_{\mathbf{k}}^{(c)}}. \tag{11}$$

The features of the scattering matrix $\Gamma(\mathbf{k}, \omega)$ in Equation (7) can be read from Figure 1. Figure 1 shows the spectral function of Γ defined as $A_T(0, \omega) = -\text{Im}\Gamma(0, \omega)$ as a function of ω for $\alpha = 2$ (red) and $\alpha = 0.5$ (black). For clarity, we show the spectral function for the same parameters in logarithmic scale. The scattering matrix is formed by a sharp and real pole at the energy of the bound state (narrow peak) and a continuum of excitations at $\omega > 0$ only visible in the inset. As α is increased from large negative values, the bound state becomes well-defined leading to a sharper pole.

Turning our attention to many-body physics, we have that in the limit $g_{BB} \rightarrow 0$ for a non-interacting BEC, Equation (7) reads as

$$\Sigma(\mathbf{k}, \omega) = n \frac{4\pi}{m} \frac{1}{\ln\left(\frac{\omega - \frac{k^2}{4m}}{\epsilon_B}\right)}, \tag{12}$$

which is independent of the cut-off Λ as discussed. For non-zero g_{BB} , we obtain Equation (9) numerically. In practice, however, we will only study a weakly interacting BEC.

Before delving into the numerical details, let us comment on the approximations we have made so far. The NSCT is a non-perturbative approach that allows inclusion of the relevant Feshbach physics that may become dominant in the formation of the polaron when the interaction strength is driven towards the strongly interacting regime. This method extends far beyond the so-called Fröhlich model, allowing the impurity to form a bound state with a majority boson. The NSCT has demonstrated success in providing an explanation for the first generation of Fermi and Bose polaron experiments in atomic gases.

Moreover, the flexibility of this approach has facilitated its extension to finite temperature polarons [24], polaron-polaron interactions [37,38], Efimov physics [98,99], and remarkably, it has proven to be a valuable framework to explain polaron physics in the context of solid-state systems such as Fermi polaron-polaritons [67], and Bose polaron-polaritons [80,82]. On the other hand, the NSCT is restricted to permit the binding of a single boson to the impurity, limiting the formation of bosonic clusters around the impurity [25], and assumes that the Bogoliubov theory remains valid. Different studies have tried to improve upon the inherent restrictions of the NSCT. However, many aspects of the Bose polaron remain under debate, aspects that lie beyond the scope of this study. In this work, we keep in mind the scope and validity of our assumptions and discuss comparisons made against other approaches.

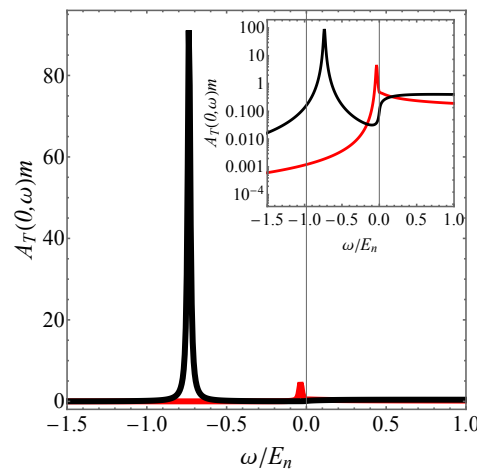


Figure 1. Spectral function $A_T(0, \omega)$ for $\alpha = 2$ (red) and $\alpha = 0.5$ (black). Spectral function $A_T(0, \omega)$ in logarithmic scale (inset). The main peak corresponds to the bound state, whereas a continuum of excitations appear for $\omega > 0$.

2.2. Quasiparticle Properties

The impurity Green’s function gives access to the quasiparticle properties of the polaron. In fact, the poles of the Green’s function are connected to the presence of quasiparticle states. In the vicinity of a pole, the impurity Green’s function is well approximated by [97]

$$\mathcal{G}(\mathbf{k}, \omega) \approx \frac{Z_{\mathbf{k}}}{\omega - E_{\mathbf{k}} + i\gamma_{\mathbf{k}}}, \tag{13}$$

where, $E_{\mathbf{k}}$ is the polaron energy, $Z_{\mathbf{k}}$ is the quasiparticle residue, and $\gamma_{\mathbf{k}}$ is the damping rate.

The self-consistent equation for the energy is

$$\text{Re}[\mathcal{G}^{-1}(\mathbf{k}, E_{\mathbf{k}})] = E_{\mathbf{k}} - \epsilon_{\mathbf{k}}^{(c)} - \text{Re}[\Sigma(\mathbf{k}, E_{\mathbf{k}})] = 0. \tag{14}$$

The quasiparticle residue is found from

$$Z_{\mathbf{k}}^{-1} = \left(1 - \frac{\partial \text{Re}[\Sigma(\mathbf{k}, E_{\mathbf{k}})]}{\partial \omega} \right) \Big|_{\omega=E_{\mathbf{k}}}, \tag{15}$$

while the damping rate of the polaron is given by

$$\gamma_{\mathbf{k}} = -Z_{\mathbf{k}} \text{Im}[\Sigma(\mathbf{k}, E_{\mathbf{k}})]. \tag{16}$$

The spectral function $A(\mathbf{k}, \omega)$ is normalized to one,

$$\frac{1}{2\pi} \int_{-\infty}^{\infty} d\omega A(\mathbf{k}, \omega) = 1. \tag{17}$$

For $\gamma_{\mathbf{k}} = 0$ the spectral function can be decomposed as $A(\mathbf{k}, \omega) \approx Z_{\mathbf{k}}\delta(\omega - E_{\mathbf{k}}) + I_{\text{inc}}(\mathbf{k}, \omega)$. That is, the spectral function is the sum of a coherent part (the quasiparticle) and an incoherent part $I_{\text{inc}}(\mathbf{k}, \omega)$. In the literature, these two parts are often defined to express the quasiparticle state and incoherent part to Equation (17).

Finally, the mobility of the quasiparticle can be understood in terms of an effective mass defined as

$$m_{\mathbf{k}}^* = \frac{k}{\frac{\partial E_{\mathbf{k}}}{\partial k}}. \tag{18}$$

A quasiparticle is well-defined given that the energy remains larger than its damping rate. Moreover, the quasiparticle residue $Z_{\mathbf{k}}$ is required to be large enough to be experimentally observable.

2.3. Zero-Momentum Properties

We are now in a position to study the properties of a zero-momentum impurity coupled to a Bose–Einstein condensate. In Figure 2, we show the spectral function of the impurity. We consider a weakly interacting BEC with $ng_{BB}/E_n = 0.3$. Figure 2a shows the spectral function $A(\mathbf{k} = 0, \omega)$ as a function of α and ω for a zero-momentum impurity. Figure 2b illustrates cross-sections of $A(0, \omega)$ for fixed values of α .

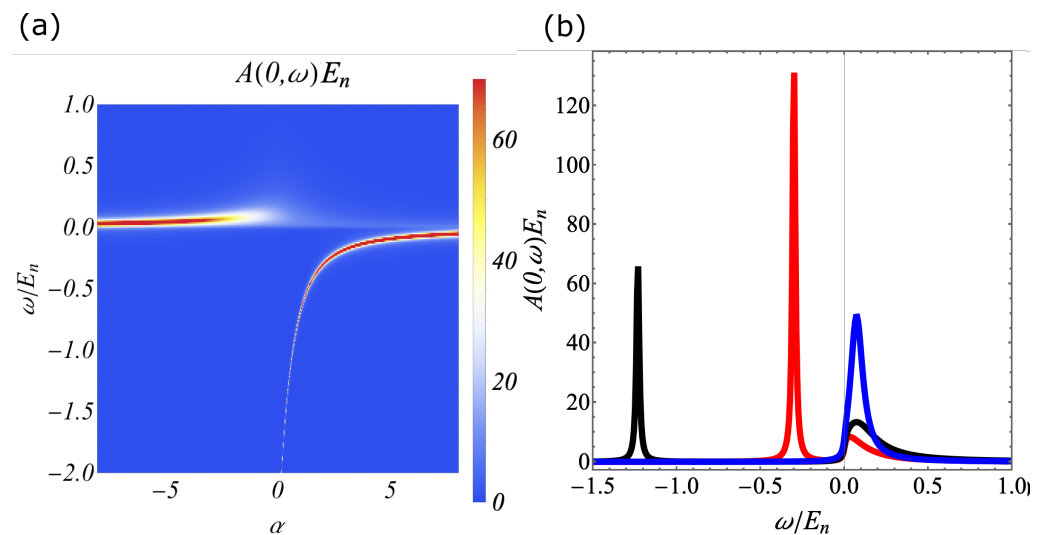


Figure 2. (a) Spectral function of a two-dimensional impurity at zero momentum as a function of ω and α . The coherent excitations (quasiparticle) are situated at the narrow maxima of the spectral function (red regions), whereas the incoherent parts of the spectral function correspond to the white regions at positive energies. (b) Spectral function for fixed $\alpha = 2$ (red), $\alpha = 0.5$ (black) and for $\alpha = -2$ (blue) and varying ω .

In Figure 2a, we observe that for large positive α an attractive polaron branch with $E_{\mathbf{k}=0} < 0$ is visible taking most of the spectral weight. This is also shown in Figure 2b where for $\alpha = 2$ a sharp peak appears at negative energies accompanied by a small bump at positive energies. This bump is formed by a continuum of incoherent excitations and is usually termed simply as the *continuum*. With decreasing $\alpha \rightarrow 0^+$, this quasiparticle peak loses visibility, while a significant increment of the spectral weight at positive energies occurs simultaneously. For negative α , a repulsive polaron branch emerges at positive energies. This quasiparticle state is formed from the spectral weight transferred from low- to high-energy excitations, as shown in Figure 2b. Here, the bump has evolved into a quasiparticle state. The repulsive polaron is a metastable state, and is much broader than the attractive polaron. In our numerics, we have added a small imaginary width of $i\eta/E_n = 0.01$ to add visibility to the attractive polaron. Here, a consequence of the NSCT

approximation is the gap opened between the attractive polaron peak and the continuum of excitations with $\omega > 0$ which is unphysical, a self-consistent treatment would lead to a continuum of excitation starting just above the polaron peak [25]. We remark that the ground state of the system is the attractive polaron even for large negative α ; however, this state loses residue and is no longer visible.

To give quantitative understanding of the polaron states, we now study the quasi-particle properties of the polaron. The energies of the attractive and repulsive polaron are plotted in Figure 3a and correspond to the peaks of the spectral function in Figure 2a. The black line gives the energy of the attractive polaron that evolves from a weakly to a strongly interacting polaron with visible energy shifts as parameter α is varied from large positive to smaller values. The repulsive polaron has positive energies. For large negative α , this is a weakly interacting state with energy slightly above zero. As $\alpha \rightarrow 0^-$, the energy of the repulsive polaron increases until the polaron ceases to exist. We are no longer able to find a solution to Equation (14) when: (a) the broadening of the spectral function becomes comparable to its energy shifts and (b) the quasiparticle residue becomes too small, which will subsequently be discussed.

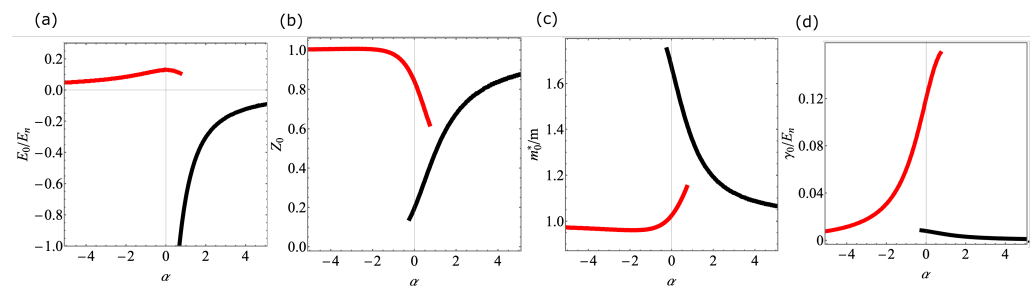


Figure 3. Zero-momentum quasiparticle properties of the two-dimensional polaron: (a) Energy $E_{\mathbf{k}=0}$, (b) Quasiparticle residue $Z_{\mathbf{k}=0}$, (c) Effective mass $m_{\mathbf{k}=0}^*/m$ and (d) Damping rate of the polaron. The red lines correspond to the repulsive branch, whereas the black lines depict the attractive polaron. System parameters are as in Figure 1.

The narrowing and broadening of the polaron branches in Figure 2a can be understood in terms of the quasiparticle properties. In Figure 3b, we plot the quasiparticle residue for the attractive and repulsive polaron. For large positive α , the attractive polaron takes most of the spectral weight. As α decreases, the residue of the polaron significantly reduces, close to $\alpha = 0$ this branch has already lost most of its quasiparticle character as $Z_0 \ll 1$. Finally, for negative α it is no longer possible to regard this branch as a quasiparticle state. Our inability to find quasiparticle states with a very small residue implies that these states become experimentally inaccessible. Through experimentation, one can extract the quasiparticle properties with spectroscopic and interferometric measurements. States with very small residue provide no visible signal [16].

The broadening of the polaron is associated with its damping rate, in this case, the attractive polaron branch is long-lived as it represents the ground state and cannot decay. On the other hand, the repulsive polaron is an excited state and has an associated finite lifetime. In Figure 3c, we illustrate the damping rate of the repulsive polaron. For large negative α , this branch has only a small broadening and is long-lived, and with increasing α the repulsive branch broadens leading to a short-lived polaron. Eventually, the broadening of the polaron exceeds its energy and it becomes no longer possible to define a repulsive polaron.

Finally, in Figure 3c we show the effective mass for the polaron states. With our approximations, we find that the attractive polaron can bind with a boson of the medium, and then as it crosses $\alpha = 0$, the effective mass approaches $m_0^*/m \rightarrow 2$.

Recently, a theoretical approach based on Quantum Monte Carlo calculations has demonstrated that the polaron branches rapidly become ill-defined as $\alpha \rightarrow 0$ [89]. The NSCT calculation, as explained above, is unable to account for a dressing larger than one Bogoli-

ubov mode. Thus, it can underestimate the surrounding cloud of the impurity, while the qualitative features are in good agreement with the QMC, we obtain a larger value of the residue at strong interactions and an effective mass that remains smaller than $m_0^*/m < 2$ contrasting to the large masses predicted in Ref. [89]. These quantitative differences arise due to the restrictions imposed by NSCT approximation. On the other hand, the interplay between the finite range of the impurity-boson potential may alleviate some effects [100].

3. The Polaron in a Bose–Einstein Condensate of Polaritons

3.1. System

We now explore a different kind of Bose polaron arising as a result of the strong coupling between exciton–polaritons and itinerant electrons in a semiconductor micro-cavity. A two-dimensional semiconductor monolayer is confined in a high-finesse cavity. Cavity photons are circularly polarised and coherently driven into the system inducing a Bose–Einstein condensation of exciton–polaritons. We consider spin-valley selection rules such that the relevant band diagram is as illustrated in Figure 4a, thus the polariton BEC only populates the valley at crystal momentum $-K$. A small fraction of itinerant electrons populate the opposite valley forming a spin-polarized two-dimensional electron gas (2DEG).

The Hamiltonian of the system is given by $\hat{H} = \hat{H}_P + \hat{H}_e + \hat{H}_{e-x}$ where

$$\hat{H}_P = \sum_{\mathbf{k}} (\epsilon_{\mathbf{k}\downarrow}^{(x)} \hat{x}_{\mathbf{k}\downarrow}^\dagger \hat{x}_{\mathbf{k}\downarrow} + \epsilon_{\mathbf{k}\downarrow}^{(a)} \hat{a}_{\mathbf{k}\downarrow}^\dagger \hat{a}_{\mathbf{k}\downarrow}) + \Omega \sum_{\mathbf{k}} (\hat{x}_{\mathbf{k}\downarrow}^\dagger \hat{a}_{\mathbf{k}\downarrow} + \hat{x}_{\mathbf{k}\downarrow} \hat{a}_{\mathbf{k}\downarrow}^\dagger) + \frac{g_{xx}}{2\mathcal{A}} \sum_{\mathbf{k}, \mathbf{k}', \mathbf{q}} \hat{x}_{\mathbf{k}+\mathbf{q}\downarrow}^\dagger \hat{x}_{\mathbf{k}'-\mathbf{q}\downarrow}^\dagger \hat{x}_{\mathbf{k}'\downarrow} \hat{x}_{\mathbf{k}\downarrow}. \quad (19)$$

We assume a valley-exciton-locked selection rule such that exciton in valley index $-K$ only couple cavity photons with left circular polarization $\sigma = \downarrow$. Here, $\hat{x}_{\mathbf{k}\downarrow}^\dagger$ creates an exciton in the valley $-K$ with in-plane momentum \mathbf{k} and energy $\epsilon_{\mathbf{k}\downarrow}^{(x)} = \omega_x + k^2/2m_x$, with m_x and ω_x the mass and energy of the excitons, respectively. Near the valleys, the dispersion of excitons is parabolic. On the other hand, $\hat{a}_{\mathbf{k}\downarrow}^\dagger$ creates a cavity photon with left circular polarization $\sigma = \downarrow$ and in-plane momentum \mathbf{k} and energy $\epsilon_{\mathbf{k}\downarrow}^{(a)} = \omega_c + k^2/2m_c$. We introduce δ , the cavity detuning from the exciton $\delta = \omega_x - \omega_c$. Finally, m_c is the mass of the cavity photons. The coupling between excitons and photons is taken within the rotating wave approximation (RWA) and is characterised by the Rabi coupling energy Ω . The RWA is justified for a large ratio ω_x/Ω such that it is safe to neglect the anti-resonant terms in the light–matter Hamiltonian. The exciton–exciton interactions are assumed to be weak and described by a short-ranged potential that is approximated by a contact interaction. This assumption is well-justified for tightly bound excitons [101].

On the eigenbasis of \hat{H}_P , neglecting the exciton–exciton interactions, the Hamiltonian can be written in terms of the lower- and upper-polaritons as

$$\hat{H}_P = \sum_{\mathbf{k}} \omega_{\mathbf{k}\downarrow}^{LP} \hat{L}_{\mathbf{k}\downarrow}^\dagger \hat{L}_{\mathbf{k}\downarrow} + \omega_{\mathbf{k}\downarrow}^{UP} \hat{U}_{\mathbf{k}\downarrow}^\dagger \hat{U}_{\mathbf{k}\downarrow}, \quad (20)$$

where $\hat{L}_{\mathbf{k}\downarrow}^\dagger$ ($\hat{U}_{\mathbf{k}\downarrow}^\dagger$) creates a lower- (upper-) polariton with energy

$$\omega_{\mathbf{k}\downarrow}^{LP/UP} = \frac{1}{2} \left(\epsilon_{\mathbf{k}\downarrow}^{(x)} + \epsilon_{\mathbf{k}\downarrow}^{(a)} \mp \sqrt{(\epsilon_{\mathbf{k}\downarrow}^{(x)} - \epsilon_{\mathbf{k}\downarrow}^{(a)})^2 + 4\Omega^2} \right). \quad (21)$$

Here, we treat the excitons and polaritons as point bosons.

The itinerant electrons are injected into the system and can be described by $\hat{H}_e = \sum_{\mathbf{k}} \epsilon_{\mathbf{k}\uparrow}^{(e)} \hat{e}_{\mathbf{k}\uparrow}^\dagger \hat{e}_{\mathbf{k}\uparrow}$, where $\epsilon_{\mathbf{k}\uparrow}^{(e)} = \omega_e + k^2/2m_e$ is the energy of an electron in the valley $+K$ with spin \uparrow . Here, the spin-valley locking prevents electrons with spin down in the valley $+K$ [102,103]. The energy of an electron at the bottom of the conduction band is denoted by $\omega_{e\uparrow}$, while $\hat{e}_{\mathbf{k}\uparrow}^\dagger$ corresponds to the creation operator of an electron with momentum \mathbf{k} in the conduction band of valley $+K$ as illustrated in Figure 4a. Since we

consider a BEC of polaritons in the valley $-K$, itinerant electrons introduced by gating will only populate the opposite valley $+K$ due to the Pauli exclusion principle.

Finally, the interaction between electrons and excitons is described by

$$\hat{H}_{e-X} = \frac{g_{x-e}}{\mathcal{A}} \sum_{\mathbf{k}, \mathbf{k}', \mathbf{q}} \hat{x}_{\mathbf{k}+\mathbf{q}\downarrow}^\dagger \hat{e}_{\mathbf{k}'-\mathbf{q}\uparrow}^\dagger \hat{e}_{\mathbf{k}'\uparrow} \hat{x}_{\mathbf{k}\downarrow}. \quad (22)$$

The electron–exciton interaction is assumed to be short-ranged and characterized by a coupling strength g_{x-e} [70]. The exciton–electron interaction supports a bound state at an energy $\epsilon_B < 0$. This state is usually coined a trion: a charged optical excitation. The binding energy of the trion $\epsilon_B < 0$ is measured with respect to the energy of the bare pair exciton–electron, that is, $E_B = \omega_x + \omega_{e\uparrow} + \epsilon_B$.

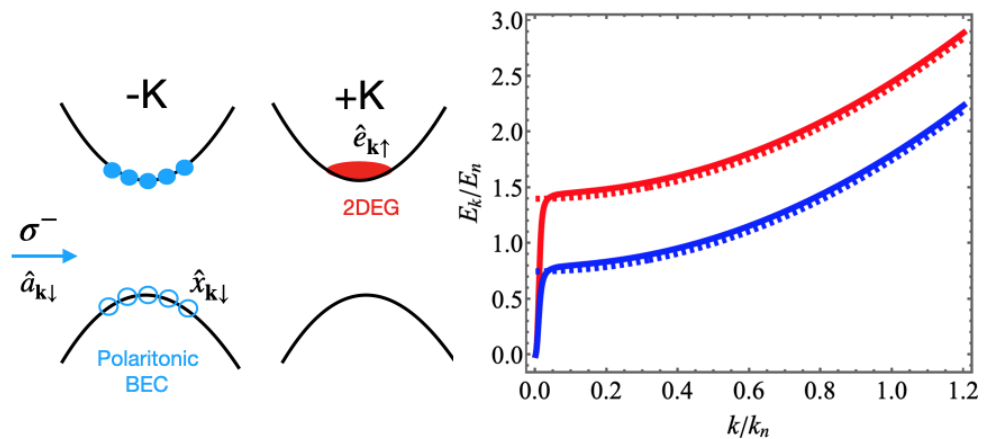


Figure 4. (Left) Relevant band structure. Exciton–polaritons are created by the coupling between cavity photons with left circular polarization \downarrow and excitons in valley $-K$. Itinerant electrons form a spin-polarized 2DEG in valley $+K$. (Right) Bogoliubov spectrum of exciton–polaritons as a function of k/k_n for $\Omega/E_n = 0.75$ and $\delta/E_n = 0$ (solid red) and $\delta/E_n = -1$ (solid blue). The dashed lines represent the parabolic dispersion of the exciton shifted by $\Delta_{LP} = -(\delta - \sqrt{\delta^2 + 4\Omega})/2$.

Contrary to atoms in ultracold gases, where the interaction can be tuned on demand by means of a magnetic Feshbach resonance, in solid-state systems, the interaction is much more fixed and cannot be varied with such flexibility. However, in semiconductor microcavities, the ability to generate hybridised light–matter quasiparticles allows for control of the interactions. In contrast to magnetic Feshbach resonances, here, the interaction can be controlled mechanically by means of a piezo-electric device [67] or by engineering of the mirrors [104] such that cavity detuning $\delta = \omega_x - \omega_c$ can be varied.

We consider a driving term $\hat{H}_{\text{pump}} = \sum_{\mathbf{k}} F \hat{a}_{\mathbf{k}\downarrow}^\dagger e^{-i\omega_p t} + \text{h.c}$ that injects photons into the cavity. Here, F is the strength of the pump and ω_p the frequency of the pump. We fix $\omega_p = \omega_{\mathbf{k}=0\downarrow}^{LP}$. The net effect of this driving term is to create a steady-state of Bose–Einstein condensation of lower polaritons of density n_{LP} with a chemical potential fixed by the pump frequency [105]. The effective Hamiltonian for the polaritons is

$$\hat{H}_P = \sum_{\mathbf{k}} E_{\mathbf{k}} \hat{\beta}_{\mathbf{k}}^\dagger \hat{\beta}_{\mathbf{k}}, \quad (23)$$

with a Bogoliubov spectrum $E_{\mathbf{k}} = \sqrt{\epsilon_{\mathbf{k}}^{LP} (\epsilon_{\mathbf{k}}^{LP} + 2C_0^2 C_{\mathbf{k}}^2 g_{xx} n_{LP})}$ and $\epsilon_{\mathbf{k}}^{LP} = \omega_{\mathbf{k}}^{LP} - \omega_0^{LP}$ [105]. Here the Hopfield coefficient $C_{\mathbf{k}}$ is

$$C_{\mathbf{k}}^2 = \frac{1}{2} \left(1 + \frac{(\epsilon_{\mathbf{k}\downarrow}^{(x)} - \epsilon_{\mathbf{k}\downarrow}^{(c)})}{\sqrt{(\epsilon_{\mathbf{k}\downarrow}^{(x)} - \epsilon_{\mathbf{k}\downarrow}^{(c)})^2 + 4\Omega^2}} \right). \quad (24)$$

The Bogoliubov dispersion is plotted in Figure 4b for $\delta/E_n = -1$ (red) and $\delta/E_n = 0$, (blue) with mass ratio $m_c/m_x = 10^{-5}$, $n_{LP}g_{xx}/E_n = 0.1$, and $\Omega/E_n = 0.75$. Here, we take $E_n = k_n^2/2m_x$ with $k_n = \sqrt{4\pi^2 n_{LP}}$. The dashed line gives the dispersions $k^2/2m_x + \Delta_{LP}$ with an effective gap $\Delta_{LP} = -(\delta - \sqrt{\delta^2 + 4\Omega})/2$ given by half the splitting of the polariton branches for a given detuning δ . This illustrates that the main effect of the light-matter coupling at large k is to induce an effective energy shift to the excitonic dispersion. The exciton and photon mix efficiently for momenta $\Delta k \lesssim \sqrt{2m_c\Omega}$. Due to the small mass of the cavity photons the coupling only occurs for $k/k_n \sim 10^{-3}$, as shown by the steep polariton dispersions in Figure 4b.

On the other hand, electrons are regarded as impurities, characterized by a density $n_e \ll n_{LP}$, such that we can assume that the BEC is unaltered in the presence of the electrons. Then, we focus on the properties of the electrons, whose Green's function is given by

$$\mathcal{G}^{-1}(\mathbf{k}, \omega) = \omega - \epsilon_{\mathbf{k}\downarrow}^{(e)} - \Sigma_e(\mathbf{k}, \omega), \tag{25}$$

written in terms of the self-energy of the electrons $\Sigma(\mathbf{k}, \omega)$. Here, again we employ the NSCT approximation

$$\Sigma_e(\mathbf{k}, \omega) = n_{LP} \mathcal{C}_0^2 \Gamma(\mathbf{k}, \omega), \tag{26}$$

where the polariton-electron scattering matrix is given by

$$\Gamma(\mathbf{k}, \omega) = \frac{1}{\frac{1}{g_{x-e}} - \Pi(\mathbf{k}, \omega)}. \tag{27}$$

The polariton–electron interaction accounts for the fact that polaritons only interact via their excitonic component. That is, the $\mathcal{C}_{\mathbf{k}=0}^2$ originates from the scattering between a condensate polariton with $\mathbf{k} = 0$ and an electron. Finally, $\Pi(\mathbf{k}, \omega)$ is the propagator of the pair exciton–electron including the light-matter coupling. In our theory the trion - the bound state between an exciton and an electron - emerges as a pole of the scattering matrix $\Gamma(\mathbf{k}, \omega)$.

3.2. Quasiparticle Properties

As explained above, we can explore Feshbach physics by varying the detuning δ . Here, we now have an interplay between the light–matter coupling Ω , the cavity detuning δ , the binding energy ϵ_B , and the density of the condensate n_{LP} . We illustrate the computed spectral function of the electrons as a function of the detuning in Figure 5 for $\Omega/|\epsilon_B| = 1$, $\Omega/E_n = 0.75$, and $m_x = 2m_e$. We note the emergence of two quasiparticle branches: an attractive and a repulsive polaron. The former takes most of the spectral weight for large negative detuning forming a weakly interacting attractive polaron. As the detuning is tuned to zero, the energy of the polaron visibly shifts towards negative values. Finally, at large positive detuning the energy of this branch saturates. On the other hand, the repulsive branch arises as a high energy state with very little spectral weight for large negative detuning. When the detuning shifts to positive values, this branch gains coherence and then vanishes for large positive detuning.

The spectral function can intuitively be explained as follows: for large negative detuning, all of the spectral weight is concentrated in the attractive polaron. This branch appears as a consequence of weak interactions between the impurity and the BEC. In this case, interactions are heavily suppressed since the BEC is essentially photonic, characterised by a very small Hopfield coefficient ($\mathcal{C}_0 \ll 1$). As the detuning is increases, excitons and photons mix giving the polaritons scope to interact via a significant excitonic component ($\mathcal{C}_0 \sim 1$). This enhances the polariton interactions and visibly shifts the energy of the attractive polaron signaling that the system is entering into the strongly interaction regime. As the cavity detuning drives to strong interactions, the spectral function exhibits two polaron branches. A high-energy polaron branch situated at positive energies with small spectral weight for

large negative detuning. It appears at positive energies due to the large value of Δ_{LP} , note that the gap is larger for negative detuning. As the detuning increases, the effective gap Δ_{LP} reduces and the coupling to the trion state becomes more efficient. This gives rise to a repulsive polaron which gains spectral weight. Finally, as the cavity detuning is varied to large positive detuning, we observe that the repulsive branch broadens losing coherence. This shows that there is an optimal value of cavity detuning, where the repulsive state is more coherent while retaining significant spectral weight.

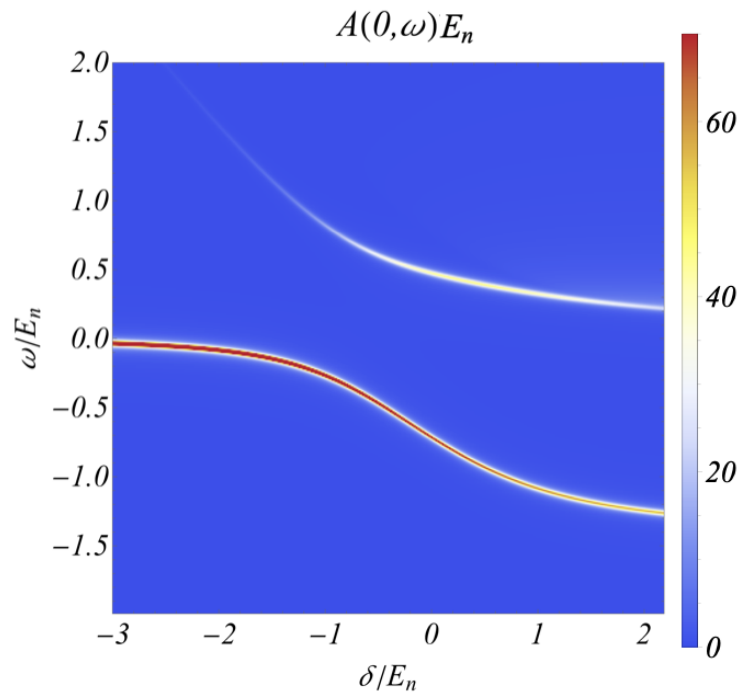


Figure 5. Spectral function for zero-momentum electrons as a function of the cavity detuning δ and ω for $\Omega/E_n = 0.75$, a coupling strength given by the binding energy $\Omega/|\epsilon_B| = 1$, and assuming non-interacting excitons $g_{xx} = 0$.

To further understand the quasiparticle properties of the system, we show in Figure 6 the energy and the residue of the polaron branches. In Figure 6a, we show the energy of the attractive (red) and repulsive polaron. The attractive polaron appears as a weakly interacting polaron state for large negative detuning as the energy shift is clearly small, in this case, the reduced interactions are a consequence of a small Hopfield factor and a trion energy that lies far away in energies. As the cavity detuning is varied to positive values, the system enters into the strongly interacting regime: the Hopfield factor of the polariton BEC enlarges and the coupling to the trion enhances. This induces large energy shifts of the attractive polaron. On the other hand, the repulsive polaron arises as a high-energy branch since the Δ_{LP} is a large positive number. Subsequently, for increasing δ , this gap reduces and the energy of the repulsive polaron decreases.

The distribution of the coherent and incoherent excitations in Figure 4b can be characterised by the quasiparticle residue of the branches. In Figure 3b, we plot the residue of the polaron states as a function of δ . When the attractive polaron (black lines) is in the weakly interacting regime, it possesses most of the spectral weight, namely $Z_0 \approx 1$. The residue of the repulsive polaron (red lines) is very small $Z_0 \ll 1$. As the system is tuned to strong interactions, the attractive polaron cedes spectral weight. This spectral weight is transferred to the repulsive polaron. Finally, while the attractive polaron remains permanently as a long-lived quasiparticle, the repulsive polaron broadens for positive detuning and becomes short-lived close to $\delta/E_n \approx 1.5$

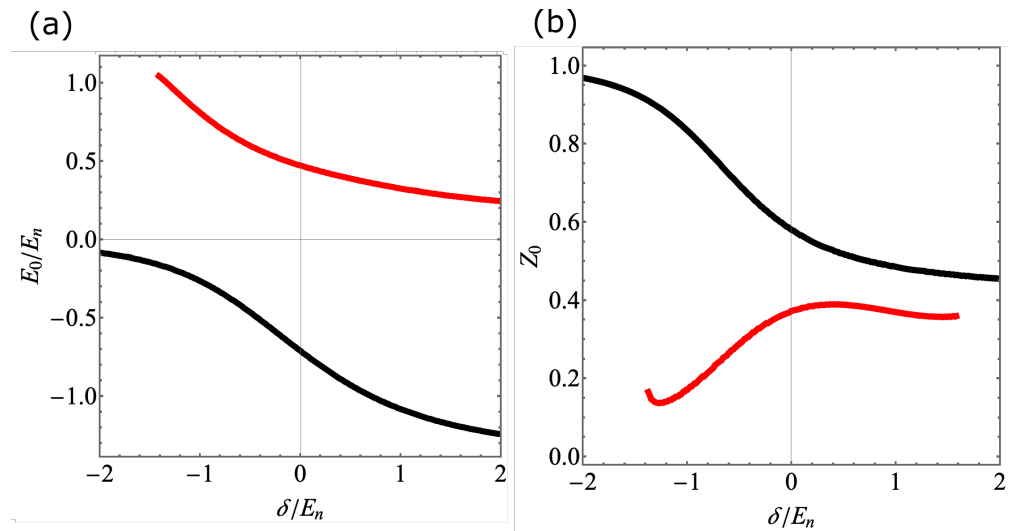


Figure 6. Quasiparticle energy and residue for zero-momentum electrons in the polariton BEC. (a) Energy of the attractive (black) and repulsive polaron (red). (b) Residue for the attractive (black) and repulsive polaron (red). The system parameters are as in Figure 5.

Finally, we mention that polaritons are intrinsically driven-dissipative systems. Here, we have neglected losses and assumed that the system is in the strong light–matter coupling regime $\Omega/\gamma_c \gg 1$ and also, that such broadening is much smaller than the binding energy $|\epsilon_B|/\gamma_c \gg 1$. Since the trion state is formed mainly from the scattering between high-momentum polaritons and an electron, and that for such processes the polariton is essentially purely exciton, the trion is thus prevented from cavity losses.

Our results show a subtle interplay between light–matter interactions and trion physics, giving rise to two polaron states on which quasiparticle properties are heavily dependent, regarding both the properties of the polaritons and energy of the trion. In view of the recent proposals to realize polariton-mediated superconductivity [91–95], our results provide a valuable guide to optimize the parameters in which electrons couple efficiently to a Bose–Einstein condensate of polaritons.

4. Conclusions

Recent breakthrough experiments with ultracold gases and microcavity polaritons have defied the old paradigms of the polaron, taking this concept to a new frontier. Our understanding has undergone significant improvements owing to the parallel development of new theoretical and numerical approaches. Consequently, these novel approaches have allowed us to characterize the many facets of the Bose polaron. Herein, we have studied the coupling between a quantum impurity and a bosonic bath in two different scenarios, employing a diagrammatic approach based on the T-matrix approximation.

First, we examined the spectral and quasiparticle properties of an impurity coupled to an atomic BEC in two-dimensions, revealing the interplay between a repulsive and an attractive polaron as a function of the impurity-boson coupling strength. We showed that when the binding energy is far smaller or larger than the typical atomic energies, the spectral weight is mainly taken by a single polaron branch: the attractive or repulsive polaron. An interplay between these branches arises when the bound-state energy is of the order of the other relevant energies, leading to large changes of their quasiparticle properties. Second, we analyzed the coupling of itinerant electrons coupled to a polariton BEC in a semiconductor monolayer in a microcavity. Here, we employ the cavity detuning as a mechanism to explore the effects of light–matter coupling and Feshbach physics on the emergence of the polaron branches.

Although the Bose polaron has now been studied using numerous different setups, the properties of two-dimensional Bose polarons remain relatively unexplored. Therefore, our study may provide a valuable benchmark for further experiments and theo-

ries to analyse other aspects of the polaron in two-dimensions, which have so far only been characterized for three-dimensional Bose polarons, such as the orthogonality catastrophe [30,31,34], Efimov physics [33,98,99], few-body states [22,32] polaron–polaron interactions [35,37,38,106], long-ranged interactions [47–49], finite range corrections [100], Cherenkov physics and impurity dynamics [107–109], among others. The interesting effects that have been thoroughly characterised for 3D Bose polarons remain yet to be understood, in the contexts of both atomic and condensed matter.

Author Contributions: Conceptualization, A.C.-G.; writing—original draft preparation, L.F.C.-C. and A.C.-G.; writing—review and editing, L.F.C.-C. and A.C.-G. All authors have read and agreed to the published version of the manuscript.

Funding: A. C. G. acknowledges financial support from Grant UNAM DGAPA PAPIIT No. IN108620.

Informed Consent Statement: Not applicable.

Data Availability Statement: Data available upon request to the corresponding author.

Acknowledgments: We thank R. Paredes for the reading of our manuscript.

Conflicts of Interest: The authors declare no conflict of interest.

References

- Landau, L.; Pekar, S. Effective mass of a polaron. *J. Exp. Theor. Phys.* **1948**, *18*, 419–423.
- Pekar, S. Theory of electromagnetic waves in a crystal with excitons. *J. Phys. Chem. Solids* **1958**, *5*, 11–22. [[CrossRef](#)]
- Schirotzek, A.; Wu, C.H.; Sommer, A.; Zwierlein, M.W. Observation of Fermi polarons in a tunable Fermi liquid of ultracold atoms. *Phys. Rev. Lett.* **2009**, *102*, 230402. [[CrossRef](#)]
- Kohstall, C.; Zaccanti, M.; Jag, M.; Trenkwalder, A.; Massignan, P.; Bruun, G.M.; Schreck, F.; Grimm, R. Metastability and coherence of repulsive polarons in a strongly interacting Fermi mixture. *Nature* **2012**, *485*, 615–618. [[CrossRef](#)]
- Koschorreck, M.; Pertot, D.; Vogt, E.; Fröhlich, B.; Feld, M.; Köhl, M. Attractive and repulsive Fermi polarons in two dimensions. *Nature* **2012**, *485*, 619–622. [[CrossRef](#)]
- Zhang, Y.; Ong, W.; Arakelyan, I.; Thomas, J. Polaron-to-polaron transitions in the radio-frequency spectrum of a quasi-two-dimensional Fermi gas. *Phys. Rev. Lett.* **2012**, *108*, 235302. [[CrossRef](#)]
- Cetina, M.; Jag, M.; Lous, R.S.; Walraven, J.T.; Grimm, R.; Christensen, R.S.; Bruun, G.M. Decoherence of impurities in a fermi sea of ultracold atoms. *Phys. Rev. Lett.* **2015**, *115*, 135302. [[CrossRef](#)]
- Massignan, P.; Zaccanti, M.; Bruun, G.M. Polarons, dressed molecules and itinerant ferromagnetism in ultracold Fermi gases. *Rep. Prog. Phys.* **2014**, *77*, 034401. [[CrossRef](#)]
- Levinsen, J.; Parish, M.M. Strongly interacting two-dimensional Fermi gases. *Annu. Rev. Cold Atoms Mol.* **2015**, *3*, 1–75.
- Cetina, M.; Jag, M.; Lous, R.S.; Fritsche, I.; Walraven, J.T.; Grimm, R.; Levinsen, J.; Parish, M.M.; Schmidt, R.; Knap, M.; et al. Ultrafast many-body interferometry of impurities coupled to a Fermi sea. *Science* **2016**, *354*, 96–99. [[CrossRef](#)]
- Scazza, F.; Valtolina, G.; Massignan, P.; Recati, A.; Amico, A.; Burchianti, A.; Fort, C.; Inguscio, M.; Zaccanti, M.; Roati, G. Repulsive Fermi polarons in a resonant mixture of ultracold Li 6 atoms. *Phys. Rev. Lett.* **2017**, *118*, 083602. [[CrossRef](#)]
- Adlong, H.S.; Liu, W.E.; Scazza, F.; Zaccanti, M.; Oppong, N.D.; Fölling, S.; Parish, M.M.; Levinsen, J. Quasiparticle lifetime of the repulsive Fermi polaron. *Phys. Rev. Lett.* **2020**, *125*, 133401. [[CrossRef](#)]
- Fritsche, I.; Baroni, C.; Dobler, E.; Kirilov, E.; Huang, B.; Grimm, R.; Bruun, G.M.; Massignan, P. Stability and breakdown of Fermi polarons in a strongly interacting Fermi–Bose mixture. *Phys. Rev. A* **2021**, *103*, 053314. [[CrossRef](#)]
- Scazza, F.; Zaccanti, M.; Massignan, P.; Parish, M.M.; Levinsen, J. Repulsive Fermi and Bose Polarons in Quantum Gases. *Atoms* **2022**, *10*, 55. [[CrossRef](#)]
- Hu, M.G.; Van de Graaff, M.J.; Kedar, D.; Corson, J.P.; Cornell, E.A.; Jin, D.S. Bose polarons in the strongly interacting regime. *Phys. Rev. Lett.* **2016**, *117*, 055301. [[CrossRef](#)]
- Jørgensen, N.B.; Wacker, L.; Skalmstang, K.T.; Parish, M.M.; Levinsen, J.; Christensen, R.S.; Bruun, G.M.; Arlt, J.J. Observation of attractive and repulsive polarons in a Bose–Einstein condensate. *Phys. Rev. Lett.* **2016**, *117*, 055302. [[CrossRef](#)]
- Ardila, L.P.; Jørgensen, N.; Pohl, T.; Giorgini, S.; Bruun, G.; Arlt, J. Analyzing a Bose polaron across resonant interactions. *Phys. Rev. A* **2019**, *99*, 063607. [[CrossRef](#)]
- Skou, M.G.; Skov, T.G.; Jørgensen, N.B.; Nielsen, K.K.; Camacho-Guardian, A.; Pohl, T.; Bruun, G.M.; Arlt, J.J. Non-equilibrium quantum dynamics and formation of the Bose polaron. *Nat. Phys.* **2021**, *17*, 731–735. [[CrossRef](#)]
- Yan, Z.Z.; Ni, Y.; Robens, C.; Zwierlein, M.W. Bose polarons near quantum criticality. *Science* **2020**, *368*, 190–194. [[CrossRef](#)]
- Li, W.; Sarma, S.D. Variational study of polarons in Bose–Einstein condensates. *Phys. Rev. A* **2014**, *90*, 013618. [[CrossRef](#)]
- Christensen, R.S.; Levinsen, J.; Bruun, G.M. Quasiparticle Properties of a Mobile Impurity in a Bose–Einstein Condensate. *Phys. Rev. Lett.* **2015**, *115*, 160401. [[CrossRef](#)] [[PubMed](#)]

22. Shchadilova, Y.E.; Schmidt, R.; Grusdt, F.; Demler, E. Quantum Dynamics of Ultracold Bose Polarons. *Phys. Rev. Lett.* **2016**, *117*, 113002. [[CrossRef](#)] [[PubMed](#)]
23. Levinsen, J.; Parish, M.M.; Christensen, R.S.; Arlt, J.J.; Bruun, G.M. Finite-temperature behavior of the Bose polaron. *Phys. Rev. A* **2017**, *96*, 063622. [[CrossRef](#)]
24. Guenther, N.E.; Massignan, P.; Lewenstein, M.; Bruun, G.M. Bose polarons at finite temperature and strong coupling. *Phys. Rev. Lett.* **2018**, *120*, 050405. [[CrossRef](#)] [[PubMed](#)]
25. Rath, S.P.; Schmidt, R. Field-theoretical study of the Bose polaron. *Phys. Rev. A* **2013**, *88*, 053632. [[CrossRef](#)]
26. Field, B.; Levinsen, J.; Parish, M.M. Fate of the Bose polaron at finite temperature. *Phys. Rev. A* **2020**, *101*, 013623. [[CrossRef](#)]
27. Ardila, L.P.; Giorgini, S. Impurity in a Bose–Einstein condensate: Study of the attractive and repulsive branch using quantum Monte Carlo methods. *Phys. Rev. A* **2015**, *92*, 033612. [[CrossRef](#)]
28. Grusdt, F.; Seetharam, K.; Shchadilova, Y.; Demler, E. Strong-coupling Bose polarons out of equilibrium: Dynamical renormalization-group approach. *Phys. Rev. A* **2018**, *97*, 033612. [[CrossRef](#)]
29. Drescher, M.; Salmhofer, M.; Enss, T. Theory of a resonantly interacting impurity in a Bose–Einstein condensate. *Phys. Rev. Res.* **2020**, *2*, 032011. [[CrossRef](#)]
30. Massignan, P.; Yegovtsev, N.; Gurarie, V. Universal Aspects of a Strongly Interacting Impurity in a Dilute Bose Condensate. *Phys. Rev. Lett.* **2021**, *126*, 123403. [[CrossRef](#)]
31. Guenther, N.E.; Schmidt, R.; Bruun, G.M.; Gurarie, V.; Massignan, P. Mobile impurity in a Bose–Einstein condensate and the orthogonality catastrophe. *Phys. Rev. A* **2021**, *103*, 013317. [[CrossRef](#)]
32. Christianen, A.; Cirac, J.I.; Schmidt, R. Chemistry of a Light Impurity in a Bose–Einstein Condensate. *Phys. Rev. Lett.* **2022**, *128*, 183401. [[CrossRef](#)] [[PubMed](#)]
33. Christianen, A.; Cirac, J.I.; Schmidt, R. Bose polaron and the Efimov effect: A Gaussian-state approach. *Phys. Rev. A* **2022**, *105*, 053302. [[CrossRef](#)]
34. Yegovtsev, N.; Massignan, P.; Gurarie, V. Strongly interacting impurities in a dilute Bose condensate. *Phys. Rev. A* **2022**, *106*, 033305. [[CrossRef](#)]
35. Naidon, P. Two Impurities in a Bose–Einstein Condensate: From Yukawa to Efimov Attracted Polarons. *J. Phys. Soc. Jpn.* **2018**, *87*, 043002. [[CrossRef](#)]
36. Dehkharghani, A.S.; Volosniev, A.G.; Zinner, N.T. Coalescence of Two Impurities in a Trapped One-dimensional Bose Gas. *Phys. Rev. Lett.* **2018**, *121*, 080405. [[CrossRef](#)]
37. Camacho-Guardian, A.; Peña Ardila, L.A.; Pohl, T.; Bruun, G.M. Bipolarons in a Bose–Einstein Condensate. *Phys. Rev. Lett.* **2018**, *121*, 013401. [[CrossRef](#)]
38. Camacho-Guardian, A.; Bruun, G.M. Landau Effective Interaction between Quasiparticles in a Bose–Einstein Condensate. *Phys. Rev. X* **2018**, *8*, 031042. [[CrossRef](#)]
39. Huber, D.; Hammer, H.W.; Volosniev, A.G. In-medium bound states of two bosonic impurities in a one-dimensional Fermi gas. *Phys. Rev. Res.* **2019**, *1*, 033177. [[CrossRef](#)]
40. Deng, F.L.; Shi, T.; Yi, S. Effective interactions between two impurities in quasi-two-dimensional dipolar Bose–Einstein condensates. *Commun. Theor. Phys.* **2020**, *72*, 075501. [[CrossRef](#)]
41. Mukherjee, K.; Mistakidis, S.I.; Majumder, S.; Schmelcher, P. Induced interactions and quench dynamics of bosonic impurities immersed in a Fermi sea. *Phys. Rev. A* **2020**, *102*, 053317. [[CrossRef](#)]
42. Mistakidis, S.I.; Koutentakis, G.M.; Katsimiga, G.C.; Busch, T.; Schmelcher, P. Many-body quantum dynamics and induced correlations of Bose polarons. *New J. Phys.* **2020**, *22*, 043007. [[CrossRef](#)]
43. Will, M.; Astrakharchik, G.E.; Fleischhauer, M. Polaron Interactions and Bipolarons in One-Dimensional Bose Gases in the Strong Coupling Regime. *Phys. Rev. Lett.* **2021**, *127*, 103401. [[CrossRef](#)]
44. Keiler, K.; Mistakidis, S.I.; Schmelcher, P. Polarons and their induced interactions in highly imbalanced triple mixtures. *Phys. Rev. A* **2021**, *104*, L031301. [[CrossRef](#)]
45. Theel, F.; Mistakidis, S.I.; Keiler, K.; Schmelcher, P. Counterflow dynamics of two correlated impurities immersed in a bosonic gas. *Phys. Rev. A* **2022**, *105*, 053314. [[CrossRef](#)]
46. Ardila, L.A.P. Ultra-Dilute Gas of Polarons in a Bose–Einstein Condensate. *Atoms* **2022**, *10*. [[CrossRef](#)]
47. Ardila, L.A.P.; Pohl, T. Ground-state properties of dipolar Bose polarons. *J. Phys. B At. Mol. Opt. Phys.* **2018**, *52*, 015004. [[CrossRef](#)]
48. Astrakharchik, G.E.; Ardila, L.A.P.; Schmidt, R.; Jachymski, K.; Negretti, A. Ionic polaron in a Bose–Einstein condensate. *Commun. Phys.* **2021**, *4*, 94. [[CrossRef](#)]
49. Christensen, E.R.; Camacho-Guardian, A.; Bruun, G.M. Charged Polarons and Molecules in a Bose–Einstein Condensate. *Phys. Rev. Lett.* **2021**, *126*, 243001. [[CrossRef](#)]
50. Ding, S.; Drewsen, M.; Arlt, J.J.; Bruun, G.M. Mediated interactions between ions in quantum degenerate gases. *arXiv* **2022**, arXiv:2203.02768.
51. Astrakharchik, G.E.; Peña Ardila, L.A.; Jachymski, K.; Negretti, A. Charged impurities in a Bose–Einstein condensate: Many-body bound states and induced interactions. *arXiv* **2022**, arXiv:2206.03476.
52. Ardila, L.A.P. Monte Carlo methods for impurity physics in ultracold Bose quantum gases. *Nat. Rev. Phys.* **2022**, *4*, 214. [[CrossRef](#)]
53. Hopfield, J.J. Theory of the Contribution of Excitons to the Complex Dielectric Constant of Crystals. *Phys. Rev.* **1958**, *112*, 1555–1567. [[CrossRef](#)]

54. Amo, A.; Lefrère, J.; Pigeon, S.; Adrados, C.; Ciuti, C.; Carusotto, I.; Houdré, R.; Giacobino, E.; Bramati, A. Superfluidity of polaritons in semiconductor microcavities. *Nat. Phys.* **2009**, *5*, 805–810. [[CrossRef](#)]
55. Deng, H.; Haug, H.; Yamamoto, Y. Exciton-polariton Bose–Einstein condensation. *Rev. Mod. Phys.* **2010**, *82*, 1489–1537. [[CrossRef](#)]
56. Daskalakis, K.S.; Maier, S.A.; Murray, R.; Kéna-Cohen, S. Nonlinear interactions in an organic polariton condensate. *Nat. Mater.* **2014**, *13*, 271–278. [[CrossRef](#)]
57. Lagoudakis, K.G.; Wouters, M.; Richard, M.; Baas, A.; Carusotto, I.; André, R.; Dang, L.S.; Deveaud-Plédran, B. Quantized vortices in an exciton–polariton condensate. *Nat. Phys.* **2008**, *4*, 706–710. [[CrossRef](#)]
58. Sanvitto, D.; Marchetti, F.M.; Szymańska, M.H.; Tosi, G.; Baudisch, M.; Laussy, F.P.; Krizhanovskii, D.N.; Skolnick, M.S.; Marrucci, L.; Lemaître, A.; et al. Persistent currents and quantized vortices in a polariton superfluid. *Nat. Phys.* **2010**, *6*, 527–533. [[CrossRef](#)]
59. Rubo, Y.G. Half Vortices in Exciton Polariton Condensates. *Phys. Rev. Lett.* **2007**, *99*, 106401. [[CrossRef](#)]
60. Lagoudakis, K.G.; Ostatnický, T.; Kavokin, A.V.; Rubo, Y.G.; André, R.; Deveaud-Plédran, B. Observation of Half-Quantum Vortices in an Exciton-Polariton Condensate. *Science* **2009**, *326*, 974–976. [[CrossRef](#)]
61. Takemura, N.; Trebaol, S.; Wouters, M.; Portella-Oberli, M.T.; Deveaud, B. Polaritonic Feshbach resonance. *Nat. Phys.* **2014**, *10*, 500–504. [[CrossRef](#)]
62. Wasak, T.; Schmidt, R.; Piazza, F. Quantum-Zeno Fermi polaron in the strong dissipation limit. *Phys. Rev. Res.* **2021**, *3*, 013086. [[CrossRef](#)]
63. Tan, L.B.; Cotlet, O.; Bergschneider, A.; Schmidt, R.; Back, P.; Shimazaki, Y.; Kroner, M.; İmamoğlu, A.M.C. Interacting Polaron-Polaritons. *Phys. Rev. X* **2020**, *10*, 021011. [[CrossRef](#)]
64. Bastarrachea-Magnani, M.A.; Camacho-Guardian, A.; Bruun, G.M. Attractive and Repulsive Exciton-Polariton Interactions Mediated by an Electron Gas. *Phys. Rev. Lett.* **2021**, *126*, 127405. [[CrossRef](#)]
65. Bastarrachea-Magnani, M.A.; Thomsen, J.; Camacho-Guardian, A.; Bruun, G.M. Polaritons in an Electron Gas Quasiparticles and Landau Effective Interactions. *Atoms* **2021**, *9*, 81. [[CrossRef](#)]
66. Muir, J.B.; Levinsen, J.; Earl, S.K.; Conway, M.A.; Cole, J.H.; Wurdack, M.; Mishra, R.; David, J.; Estrecho, E.; Lu, Y.; et al. Exciton-polaron interactions in monolayer WS₂. *arXiv* **2022**, arXiv:2206.12007.
67. Sidler, M.; Back, P.; Cotlet, O.; Srivastava, A.; Fink, T.; Kroner, M.; Demler, E.; Imamoglu, A. Fermi polaron-polaritons in charge-tunable atomically thin semiconductors. *Nat. Phys.* **2017**, *13*, 255–261. [[CrossRef](#)]
68. Efimkin, D.K.; MacDonald, A.H. Exciton-polarons in doped semiconductors in a strong magnetic field. *Phys. Rev. B* **2018**, *97*, 235432. [[CrossRef](#)]
69. Efimkin, D.K.; MacDonald, A.H. Many-body theory of trion absorption features in two-dimensional semiconductors. *Phys. Rev. B* **2017**, *95*, 035417. [[CrossRef](#)]
70. Efimkin, D.K.; Laird, E.K.; Levinsen, J.; Parish, M.M.; MacDonald, A.H. Electron-exciton interactions in the exciton-polaron problem. *Phys. Rev. B* **2021**, *103*, 075417. [[CrossRef](#)]
71. Goldstein, T.; Wu, Y.C.; Chen, S.Y.; Taniguchi, T.; Watanabe, K.; Varga, K.; Yan, J. Ground and excited state exciton polarons in monolayer MoSe₂. *J. Chem. Phys.* **2020**, *153*, 071101. [[CrossRef](#)] [[PubMed](#)]
72. Ravets, S.; Knüppel, P.; Faelt, S.; Cotlet, O.; Kroner, M.; Wegscheider, W.; Imamoglu, A. Polaron polaritons in the integer and fractional quantum Hall regimes. *Phys. Rev. Lett.* **2018**, *120*, 057401. [[CrossRef](#)] [[PubMed](#)]
73. Cotlet, O.; Wild, D.S.; Lukin, M.D.; Imamoglu, A. Rotons in optical excitation spectra of monolayer semiconductors. *Phys. Rev. B* **2020**, *101*, 205409. [[CrossRef](#)]
74. Imamoglu, A.; Cotlet, O.; Schmidt, R. Exciton-polarons in two-dimensional semiconductors and the Tavis–Cummings model. *Comptes Rendus. Phys.* **2021**, *22*, 1–8. [[CrossRef](#)]
75. Cotlet, O.; Pientka, F.; Schmidt, R.; Zarand, G.; Demler, E.; Imamoglu, A. Transport of neutral optical excitations using electric fields. *Phys. Rev. X* **2019**, *9*, 041019. [[CrossRef](#)]
76. Rana, F.; Koksal, O.; Manolatou, C. Many-body theory of the optical conductivity of excitons and trions in two-dimensional materials. *Phys. Rev. B* **2020**, *102*, 085304. [[CrossRef](#)]
77. Pimenov, D.; von Delft, J.; Glazman, L.; Goldstein, M. Fermi-edge exciton-polaritons in doped semiconductor microcavities with finite hole mass. *Phys. Rev. B* **2017**, *96*, 155310. [[CrossRef](#)]
78. Shahnazaryan, V.; Kozin, V.; Shelykh, I.; Iorsh, I.; Kyriienko, O. Tunable optical nonlinearity for transition metal dichalcogenide polaritons dressed by a Fermi sea. *Phys. Rev. B* **2020**, *102*, 115310. [[CrossRef](#)]
79. Grusdt, F.; Fleischhauer, M. Tunable Polarons of Slow-Light Polaritons in a Two-Dimensional Bose–Einstein Condensate. *Phys. Rev. Lett.* **2016**, *116*, 053602. [[CrossRef](#)]
80. Levinsen, J.; Marchetti, F.M.; Keeling, J.; Parish, M.M. Spectroscopic Signatures of Quantum Many-Body Correlations in Polariton Microcavities. *Phys. Rev. Lett.* **2019**, *123*, 266401. [[CrossRef](#)]
81. Navadeh-Toupchi, M.; Takemura, N.; Anderson, M.D.; Oberli, D.Y.; Portella-Oberli, M.T. Polaritonic Cross Feshbach Resonance. *Phys. Rev. Lett.* **2019**, *122*, 047402. [[CrossRef](#)] [[PubMed](#)]
82. Bastarrachea-Magnani, M.A.; Camacho-Guardian, A.; Wouters, M.; Bruun, G.M. Strong interactions and biexcitons in a polariton mixture. *Phys. Rev. B* **2019**, *100*, 195301. [[CrossRef](#)]
83. Camacho-Guardian, A.; Nielsen, K.K.; Pohl, T.; Bruun, G.M. Polariton dynamics in strongly interacting quantum many-body systems. *Phys. Rev. Res.* **2020**, *2*, 023102. [[CrossRef](#)]

84. Camacho-Guardian, A.; Bastarrachea-Magnani, M.A.; Bruun, G.M. Mediated Interactions and Photon Bound States in an Exciton-Polariton Mixture. *Phys. Rev. Lett.* **2021**, *126*, 017401. [[CrossRef](#)] [[PubMed](#)]
85. Vashisht, A.; Richard, M.; Minguzzi, A. Bose polaron in a quantum fluid of light. *SciPost Phys.* **2022**, *12*, 008. [[CrossRef](#)]
86. Hryhorchak, O.; Panochko, G.; Pastukhov, V. Mean-field study of repulsive 2D and 3D Bose polarons. *J. Phys. B At. Mol. Opt. Phys.* **2020**, *53*, 205302. [[CrossRef](#)]
87. Casteels, W.; Tempere, J.; Devreese, J.T. Polaronic properties of an impurity in a Bose–Einstein condensate in reduced dimensions. *Phys. Rev. A* **2012**, *86*, 043614. [[CrossRef](#)]
88. Pastukhov, V. Polaron in dilute 2D Bose gas at low temperatures. *J. Phys. B: At. Mol. Opt. Phys.* **2018**, *51*, 155203. [[CrossRef](#)]
89. Ardila, L.A.P.n.; Astrakharchik, G.E.; Giorgini, S. Strong coupling Bose polarons in a two-dimensional gas. *Phys. Rev. Res.* **2020**, *2*, 023405. [[CrossRef](#)]
90. Ding, S.; Domínguez-Castro, G.A.; Julku, A.; Camacho-Guardian, A.; Bruun, G.M. Polarons and bipolarons in a two-dimensional square lattice. *arXiv* **2022**, arXiv:2212.00890.
91. Shelykh, I.A.; Taylor, T.; Kavokin, A.V. Rotons in a Hybrid Bose–Fermi System. *Phys. Rev. Lett.* **2010**, *105*, 140402. [[CrossRef](#)] [[PubMed](#)]
92. Matuszewski, M.; Taylor, T.; Kavokin, A.V. Exciton Supersolidity in Hybrid Bose–Fermi Systems. *Phys. Rev. Lett.* **2012**, *108*, 060401. [[CrossRef](#)]
93. Laussy, F.P.; Kavokin, A.V.; Shelykh, I.A. Exciton-Polariton Mediated Superconductivity. *Phys. Rev. Lett.* **2010**, *104*, 106402. [[CrossRef](#)] [[PubMed](#)]
94. Cotlet, O.; Zeytinoglu, S.; Sigrist, M.; Demler, E.; Imamoğlu, A.m.c. Superconductivity and other collective phenomena in a hybrid Bose–Fermi mixture formed by a polariton condensate and an electron system in two dimensions. *Phys. Rev. B* **2016**, *93*, 054510. [[CrossRef](#)]
95. Julku, A.; Kinnunen, J.J.; Camacho-Guardian, A.; Bruun, G.M. Light-induced topological superconductivity in transition metal dichalcogenide monolayers. *arXiv* **2022**, arXiv:2204.12229.
96. Chin, C.; Grimm, R.; Julienne, P.; Tiesinga, E. Feshbach resonances in ultracold gases. *Rev. Mod. Phys.* **2010**, *82*, 1225–1286. [[CrossRef](#)]
97. Fetter, A.; Walecka, J. *Quantum Theory of Many-Particle Systems*; Dover Books on Physics Series; Dover Publications: Mineola, NY, USA, 1971.
98. Sun, M.; Zhai, H.; Cui, X. Visualizing the Efimov Correlation in Bose Polarons. *Phys. Rev. Lett.* **2017**, *119*, 013401. [[CrossRef](#)]
99. Sun, M.; Cui, X. Enhancing the Efimov correlation in Bose polarons with large mass imbalance. *Phys. Rev. A* **2017**, *96*, 022707. [[CrossRef](#)]
100. Levinsen, J.; Ardila, L.A.P.n.; Yoshida, S.M.; Parish, M.M. Quantum Behavior of a Heavy Impurity Strongly Coupled to a Bose Gas. *Phys. Rev. Lett.* **2021**, *127*, 033401. [[CrossRef](#)]
101. Wouters, M. Resonant polariton-polariton scattering in semiconductor microcavities. *Phys. Rev. B* **2007**, *76*, 045319. [[CrossRef](#)]
102. Schaibley, J.R.; Yu, H.; Clark, G.; Rivera, P.; Ross, J.S.; Seyler, K.L.; Yao, W.; Xu, X. Valleytronics in 2D materials. *Nat. Rev. Mater.* **2016**, *1*, 1–15. [[CrossRef](#)]
103. Xu, X.; Yao, W.; Xiao, D.; Heinz, T.F. Spin and pseudospins in layered transition metal dichalcogenides. *Nat. Phys.* **2014**, *10*, 343–350. [[CrossRef](#)]
104. García Jomaso, Y.A.; Vargas, B.; Ley Dominguez, D.; Ordoñez-Romero, C.L.; Lara-García, H.A.; Camacho-Guardian, A.; Pirruccio, G. The Fate of the Upper Polariton: Breakdown of the Quasiparticle Picture in the Continuum. *arXiv* **2022**, arXiv:2209.13698.
105. Carusotto, I.; Ciuti, C. Quantum fluids of light. *Rev. Mod. Phys.* **2013**, *85*, 299–366. [[CrossRef](#)]
106. Fujii, K.; Hongo, M.; Enss, T. Universal van der Waals force between heavy polarons in superfluids. *arXiv* **2022**, arXiv:2206.01048.
107. Nielsen, K.K.; Ardila, L.A.P.; Bruun, G.M.; Pohl, T. Critical slowdown of non-equilibrium polaron dynamics. *New J. Phys.* **2019**, *21*, 043014. [[CrossRef](#)]
108. Seetharam, K.; Shchadilova, Y.; Grusdt, F.; Zvonarev, M.B.; Demler, E. Dynamical Quantum Cherenkov Transition of Fast Impurities in Quantum Liquids. *Phys. Rev. Lett.* **2021**, *127*, 185302. [[CrossRef](#)]
109. Drescher, M.; Salmhofer, M.; Enss, T. Quench Dynamics of the Ideal Bose Polaron at Zero and Nonzero Temperatures. *Phys. Rev. A* **2021**, *103*, 033317. [[CrossRef](#)]

Disclaimer/Publisher’s Note: The statements, opinions and data contained in all publications are solely those of the individual author(s) and contributor(s) and not of MDPI and/or the editor(s). MDPI and/or the editor(s) disclaim responsibility for any injury to people or property resulting from any ideas, methods, instructions or products referred to in the content.